

Full length article

Experimental residual capacity of steel-reinforced concrete-filled steel tubular stub columns after fire exposure

D. Medall^a, C. Ibáñez^{a,*}, V. Albero^b, A. Espinós^a, M.L. Romero^a^a ICITECH, Universitat Politècnica de València, Valencia, Spain^b Department of Mechanical Engineering and Construction, Universitat Jaume I, Castellón, Spain

ARTICLE INFO

Keywords:

Steel-reinforced concrete-filled steel tubular columns
 Post-fire behaviour
 Residual Strength Index
 Design equations
 Eurocode 4

ABSTRACT

Technological advances in the development of steel–concrete composite structures have led to the introduction of novel types of sections in the sought of higher load-bearing capacities. Particularly for composite columns, the axial capacity of concrete-filled steel tubular (CFST) sections may be enhanced by the introduction of an open steel profile embedded within the concrete infill, forming the so-called steel-reinforced concrete-filled steel tubular (SR-CFST) columns. An important aspect that should be revised, in order to safely use these sections in design, is their performance after a fire. In this experimental program, six SR-CFST stub columns are tested in the post-fire situation. Two series of columns comprising three circular and three square sections with the same steel usage are tested for comparison purposes. The size of the inner steel profile is varied in order to investigate its effect over the post-fire capacity of the columns. The specimens were initially exposed to elevated temperatures inside an electric furnace, and then cooled to ambient temperature; afterwards compressive axial load was applied gradually until failure, to ascertain their residual capacity. The experimental results show the high ductility of the SR-CFST stub columns after heating, with the circular specimens reaching higher post-fire peak loads than their square counterparts. This load increases with the size of the embedded steel profile. The post-fire capacities of the columns are evaluated through the Residual Strength Index, showing similar values for both circular and square SR-CFST columns. Finally, a design equation is proposed to facilitate the evaluation of the post-fire compression resistance of SR-CFST columns, as an extension of the existing room temperature design equation in Eurocode 4 Part 1–2 for CFST columns, accounting for the degradation of the steel and concrete after fire exposure through the corresponding residual factors.

1. Introduction

In recent years, innovative solutions have been developed to increase both the load-bearing capacity and fire resistance of steel–concrete composite columns, as it is the case of steel-reinforced concrete-filled steel tubular (SR-CFST) sections, where an open steel profile is embedded within the concrete infill of the well-known concrete-filled steel tubular (CFST) section. Examples of high-rise buildings which use these types of composite sections for the main load-bearing compression members are spreading around the world [1,2], in sought of higher capacities with minimum cross-sectional dimensions.

In a fire situation, this form of construction also enhances the performance of the composite columns, since the inner steel profile is thermally protected by the surrounding concrete, thus delaying its degradation at high temperatures [3]. Therefore, SR-CFST columns may be a good alternative to improve the fire resistance of CFST columns, which is limited by the direct exposure of the outer steel tube to the heat source.

Although the many advantages of the application of SR-CFST columns are making their study appealing for the research community, investigations on their fire and post-fire structural response are particularly scarce, especially those that consider the post-heating phase.

A better understanding of the behaviour of SR-CFST columns after a fire, which is dominated by the maximum temperature achieved by the different components of the composite cross-section, is required to properly estimate the residual capacity of this typology and to adopt a reasonable reinstatement strategy with minimum post-fire repair.

Revising the available literature, it is worth drawing attention to the tests performed at the University of Liège [4], those carried out in Shanghai [5,6] and the experiments conducted at Southeast University [7]. In the first experimental program, the fire resistance of ten slender composite columns was tested using self-compacting concrete. Four of the ten sections were SR-CFST (with an embedded HEB120 steel profile), combining circular and square shapes for the outer steel tube.

* Corresponding author.

E-mail address: caribus@upv.es (C. Ibáñez).

Notations

| | |
|---------------------------|---|
| b | Flange dimension of the open steel profile |
| f_c | Compressive concrete cylinder strength (test date) |
| f_{ui} | Ultimate strength of steel for the embedded steel profile |
| f_{uo} | Ultimate strength of steel for the outer steel tube |
| $f_{ui,post}$ | Ultimate strength of steel for the embedded steel profile after fire exposure |
| $f_{uo,post}$ | Ultimate strength of steel for the outer steel tube after fire exposure |
| f_{yo} | Yield strength of steel for the hollow steel tube |
| f_{yi} | Yield strength of steel for the embedded steel profile |
| h | Height of the open steel profile |
| t | Outer steel tube thickness |
| t_f | Flange thickness of the open steel profile |
| t_w | Web thickness of the open steel profile |
| A_a | Cross-sectional area of the outer steel tube |
| A_a | Cross-sectional area of the outer steel tube |
| A_a/A_{tot} | Steel ratio for the outer steel tube |
| A_c | Cross-sectional area of the concrete core |
| $A_{c,i}$ | Cross-sectional area of the -i concrete ring or layer |
| A_f | Cross-sectional area of the flanges of the embedded steel profile |
| A_{tot} | Total cross-sectional area of the column |
| A_{sp} | Cross-sectional area of the embedded steel profile |
| A_{sp}/A_{tot} | Steel ratio for the embedded steel profile |
| A_w | Cross-sectional area of the web of the embedded steel profile |
| B | Outer dimension for square sections |
| D | Outer diameter for circular sections |
| E_s | Elastic modulus of steel |
| $N_{calc,j}$ | Residual plastic resistance calculated for approach -j |
| $N_{post,exp}$ | Experimental residual load at post-fire |
| $N_{post,exp}/N_{calc,j}$ | Prediction error for approach -j in comparison with $N_{post,exp}$ |
| $N_{u,0}$ | Ultimate load at room temperature |
| RSI | Residual Strength Index |
| ϵ_v | Longitudinal strain |
| ϵ_h | Transverse strain |
| η_a, η_c | Factors related to the confinement of concrete |
| ν_s | Poisson's ratio of steel at the elastic range |
| $\bar{\lambda}$ | Relative slenderness |
| σ_v | Longitudinal stress at the outer steel tube surface |
| σ_h | Transverse stress at the outer steel tube surface |
| $\theta_{a,max}$ | Maximum temperature reached in the outer steel tube |
| $\theta_{c,i,max}$ | Maximum temperature reached in the -i concrete ring or layer |
| $\theta_{f,max}$ | Maximum temperature reached in the flanges of the embedded steel profile |

 $\theta_{w,max}$

Maximum temperature reached in the web of the embedded steel profile

Due to the application of intumescent paint in some specimens, the fire resistance times ranged from 39 up to 79 min for a load level of 0.4 and a maximum external dimension of 219.1 mm. For outer dimensions greater than 219.1 mm, a complementary numerical study was carried by means of the software SAFIR.

In the experimental programs by Meng et al. [5,6], fire resistance tests on eight SR-CFST columns were conducted. The effect of non-uniform heating was taken into consideration and, in this case, again square and circular geometries were considered. The SR-CFST columns had an embedded HW150×150 and were 1800 mm long although only the central 1200 mm were heated. The experiments revealed that the inner steel profile considerably enhanced the fire behaviour of the specimens, exceeding 240 min for the 1-side and 2-sides exposed columns. Lately, Mao et al. [7] also investigated the fire performance of SR-CFST columns but with cruciform section profiled steel. The specimens were tested under the ISO-834 standard fire curve and parameters including the shape of the outer steel tube (circular or square) or the load ratio were considered. Once more, it was found that the fire resistance of SR-CFST columns had substantial improvement compared with CFST columns.

Recently, the residual strength of SR-CFST stub columns after exposure to ISO-834 standard fire curve was assessed by Meng et al. [8] through tests on three non-uniformly heated 600 mm long square columns. The specimens were composed of an outer square steel tube of dimensions 300×300×6 mm and an inner steel profile HW150×150. The study focused on the influence of the number of sides exposed to the heating source, so the columns were 2, 3 and 4-sides exposed inside a small electric furnace, where a hysteretic pre-heat process was initially applied in order to approach the standard fire curve. Once cooled down, the columns were tested to failure to obtain their residual strength. As presumed, the residual strength of the columns decreased with the fire exposure time and a high ductility level was generally observed for the stub SR-CFST columns, since they maintained their load bearing capacity reasonably constant after reaching the peak point instead of showing a sharp drop. Expressions for the residual strength after different types of fire exposure were presented based on parametric studies.

The most recent research found in relation with the post-fire behaviour of SR-CFST columns is the work presented by Yang et al. [9] where the results of an extensive experimental program on 135 square SR-CFST columns are presented. In the research, 108 SR-CFST specimens were tested after being heated for different times and 27 kept unheated for reference. Among the conclusions drawn by the authors it may be highlighted that the inner steel section ratio is the parameter with the highest influence in the post-peak behaviour of the columns whereas the maximum temperature reached has the greatest effect on the residual bearing capacity of the columns. In their work, the authors also proposed a set of equations for the evaluation of the ultimate strength of square SR-CFST both at room temperature and after fire exposure. Despite the high number of tests performed, it must be noted that the range of geometrical variation was narrow since all of the tested specimens had the same outer dimension ($B = 200$ mm) with minor variations in the thickness of the outer tube (2.94 to 4.78 mm) and only three different embedded steel profiles.

Thus, the literature analysis confirms that the number of available fire and post-fire test results on SR-CFST columns is scarce. Therefore, in this paper, the results of a series of experiments on the behaviour of SR-CFST columns after exposure to elevated temperature are presented. The history of sectional temperatures is analysed as well as the response in terms of axial load–displacement. The failure mode of the

Table 1
Details of the specimens and test results.

| Specimen | D or B (mm) | t (mm) | $\frac{A_s}{A_{tot}}$ (%) | f_{yo} (MPa) | f_{uo} (MPa) | Inner section | $\frac{A_{sp}}{A_{tot}}$ (%) | f_{yi} (MPa) | f_{ui} (MPa) | f_c (MPa) | $N_{post,exp}$ (kN) |
|--------------|--------------------|-------------|---------------------------|-------------------|-------------------|------------------|------------------------------|-------------------|-------------------|----------------|------------------------|
| SR-CFST-C-T1 | 273 | 10 | 14.1 | 451 | 504 | HEB100 | 12.0 | 315 | 445 | 24.3 | 4799 |
| SR-CFST-C-T2 | 273 | 10 | 14.1 | 451 | 504 | HEB120 | 14.6 | 308 | 437 | 24.3 | >5000 |
| SR-CFST-C-T3 | 273 | 10 | 14.1 | 451 | 504 | HEB140 | 17.1 | 315 | 441 | 24.3 | >5000 |
| SR-CFST-S-T1 | 220 | 10 | 16.8 | 560 | 680 | HEB100 | 12.2 | 315 | 445 | 24.3 | 4153 |
| SR-CFST-S-T2 | 220 | 10 | 16.8 | 560 | 680 | HEB120 | 14.8 | 308 | 437 | 24.3 | 4615 |
| SR-CFST-S-T3 | 220 | 10 | 16.8 | 560 | 680 | HEB140 | 17.4 | 315 | 441 | 24.3 | 4896 |

Note: D and B are the outer diameter or dimension for circular and square sections respectively; t is the outer steel tube thickness; f_{yo} and f_{yi} are the yield strength of steel for the outer steel tube and inner embedded section respectively; f_{uo} and f_{ui} are the ultimate strength of steel for the outer steel tube and inner embedded section respectively; f_c is the concrete cylinder compressive strength; A_s/A_{tot} is the steel ratio for the outer steel tube (where A_s is the cross-sectional area of the outer steel tube and A_{tot} is the total cross-sectional area of the column); and A_{sp}/A_{tot} is the steel ratio for the embedded steel profile (where A_{sp} is the cross-sectional area of the embedded steel profile).

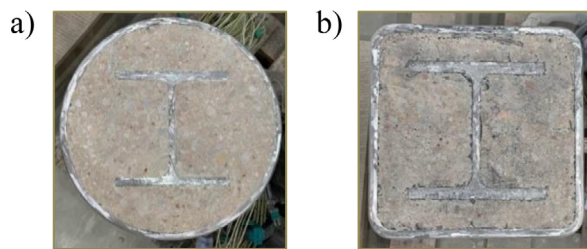


Fig. 1. SR-CFST configurations analysed: (a) circular; (b) square.

columns is investigated together with the stress state at the outer steel tube, derived from the measured strains. Finally, the suitable residual factors for steel after fire exposure are assessed, and a proposal of a design equation for the evaluation of the residual cross-sectional axial compression capacity of SR-CFST columns, based on an extension of the room temperature equations in Eurocode 4 Part 1–1, is presented.

2. Experimental investigation

2.1. Column specimens

Within the framework of this investigation, six SR-CFST specimens, consisting of three specimens with circular sections and three specimens with square sections, were fabricated to conduct axial compression loading tests after exposure to elevated temperatures (see Fig. 1a and Fig. 1b). For the sake of comparison, the selected circular and square steel tubes had the same cross-sectional steel area with a maximum difference of a 2.51%. Three different open steel sections with wide flanges are embedded inside the concrete core of both series: HEB100, HEB120 and HEB140.

Table 1 presents the cross-sectional characteristics and mechanical properties of the materials of all the specimens, and also summarizes the values of the experimental residual loads at post-fire ($N_{post,exp}$) which will be analysed in Section 2. For convenience, the test specimens were named SR-CFST-S-Ti, where S stands for the cross-sectional outer tube shape (C for circular and S for square) and Ti refers to the inner embedded steel profile dimensions, where T1 stands for HEB100, T2 for HEB120 and T3 for HEB140. As summarized in Table 1, for the circular columns, $\phi 273 \times 10$ hollow steel tubes were employed, while the hollow square steel tubes were $\#220 \times 10$ with a maximum difference of a 2.51% in cross-sectional steel area.

Note that the embedded open steel section HEB100 has an outer dimension of $h = b = 100$ mm ($t_f = 10$ mm, $t_w = 6$ mm); the HEB120 has $h = b = 120$ mm ($t_f = 11$ mm, $t_w = 6.5$ mm), and the HEB140 has $h = b = 140$ mm ($t_f = 12$ mm, $t_w = 7$ mm).

The thermal test was the first step of the experiments, where each SR-CFST specimen was uniformly exposed to high temperatures inside

the furnace. Next, after cooling at room temperature, the post-fire test to evaluate the resistance of the columns subjected to increasing axial load was conducted in a vertical frame. Test procedure is further explained in Section 2.5.

2.2. Material properties

Steel

In this experimental plan, all of the steel tubes were cold formed welded structural hollow sections in accordance with EN 10219-1 [10] and had a nominal yield strength of S355. Regarding the embedded open steel profiles, all of them were hot rolled in conformity with EN 10025-1 [11] and had a nominal yield strength of S275. To ensure getting enough material for the coupon tests, extra material than strictly needed was supplied. For all of the hollow steel tubes and embedded steel profiles that were used, the actual values of the yield strength (f_{yo} and f_{yi} , respectively) and the ultimate strength (f_{uo} and f_{ui} , respectively) are summarized in Table 1. For the steel tubes and the embedded steel profiles, the values were obtained through the corresponding coupon tests. According to the European standards, the modulus of elasticity of steel was set to 210 GPa.

Concrete

The pertinent standard tests were carried out on the 100 mm cube to obtain the actual compressive strength of concrete (f_c). Therefore, the equivalent cylinder compressive strength was obtained from the values of the strength of the cubic samples according to Eurocode 2 Part 1–1 [12], and is shown in Table 1. Concrete moisture content was 7.952% weight measured at the beginning of the experimental program. The sets of concrete samples were prepared in a planetary mixer and cured in standard conditions during 28 days. To be consistent, the corresponding concrete samples were tested the day when the experiment was conducted.

2.3. Preparation of specimens

The preparation of all of the columns as well as the tests took place at the facilities of ICITECH, Universitat Politècnica de València (Spain). To perfect the load application conditions during the post-fire test, steel plates with dimensions $300 \times 300 \times 10$ mm were placed at both ends of each specimen. First, a steel plate was welded to the bottom of the embedded steel profile (Fig. 2a). Next, the thermocouples were positioned together with the hollow steel tube in order to correctly place the thermocouples wires (Fig. 2b and Fig. 2c). For that purpose, a hole was drilled at the top end of the columns which ultimately also allowed vapour ventilation during heating. Later, the bottom of the hollow steel tube was welded to the steel plate. Once the concrete was poured into the column and settled with the help of a needle vibrator (Fig. 2d), the specimen was covered with a plastic film. Finally, the second plate was welded to the top end of the column (Fig. 2e) right after smoothing the top surface in order to assure planarity and the contact of the steel plate with all of the components.

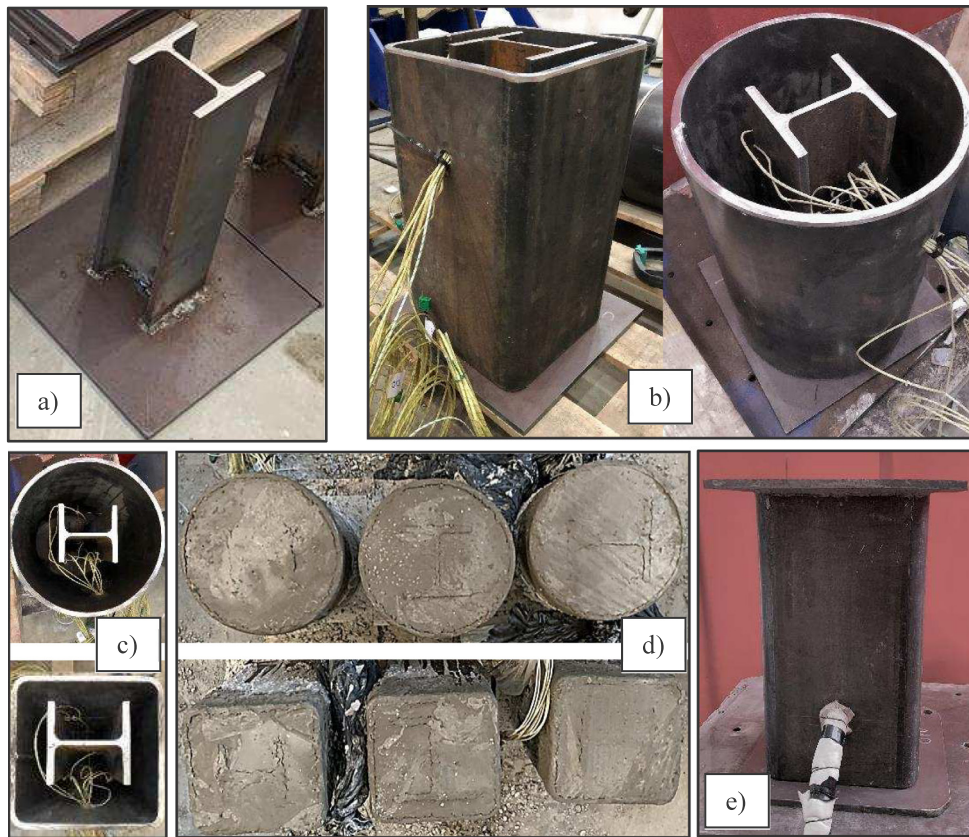


Fig. 2. Columns preparation: (a) Steel plate welded at bottom end of the embedded profile; (b) Positioning of hollow steel tube; (c) Positioning of thermocouples; (d) Columns after casting; (e) Column finished.

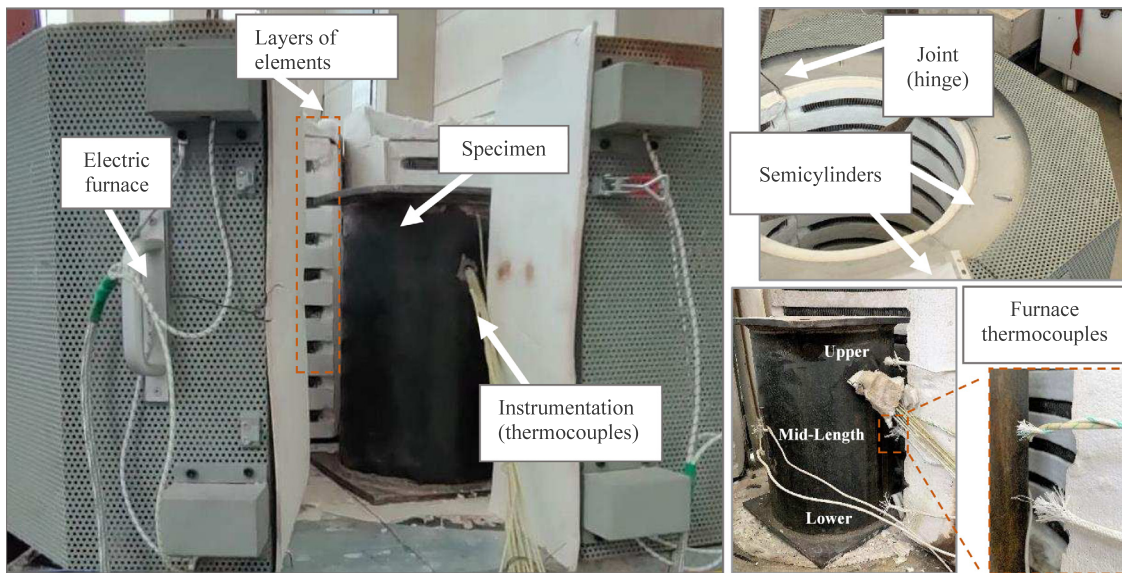


Fig. 3. Thermal test setup.

2.4. Thermal test setup

The heating of the specimens was conducted by a small vertical electric furnace of 10 kW power. The furnace consisted of two semicylinders joined by a hinge and had an inner diameter of 400 mm. As displayed in Fig. 3, on the inner refractory wall of the semicylinders, the electric elements are distributed evenly in parallel layers through the whole length for both sides.

The furnace temperature was controlled by five thermocouples located close to the refractory walls at different levels of the furnace as follow: one at the upper level, three at mid-length level and one at the lower level (see Fig. 3). For each specimen, the thermal response was registered by 12 thermocouples located at specific points of interest at the mid-length cross-section of the column, according to the layout presented in Fig. 4. Thermocouples 1 and 6 were welded to the outer surface of the steel tube whereas thermocouples 11 and 12 were welded

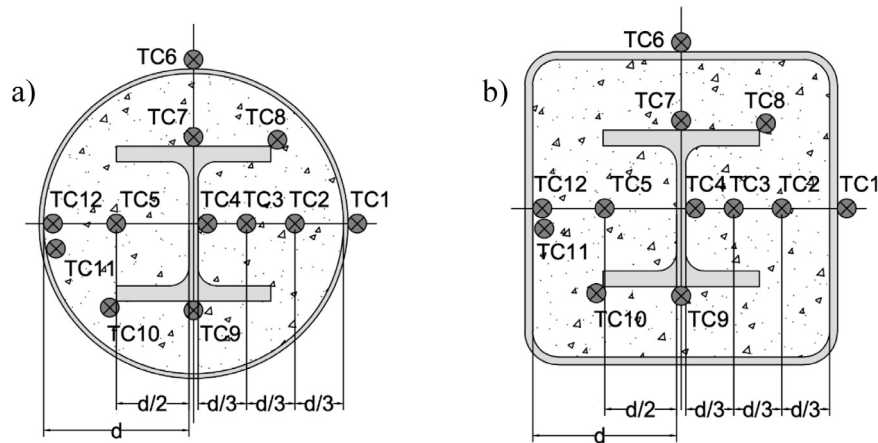


Fig. 4. Thermocouples layout: (a) circular sections; (b) square sections.

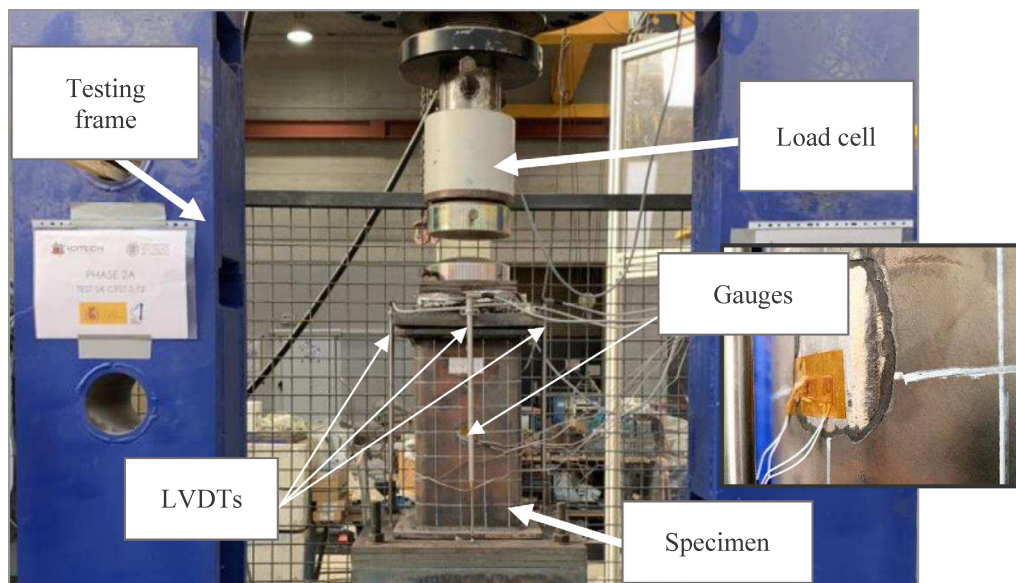


Fig. 5. Post-fire test setup.

to the inner surface. At the embedded HEB steel profile, thermocouples 7 to 10 were welded at different points of flanges and web. Thermocouples 2 to 5 were embedded in the concrete core: number 2 to 4 were placed equidistantly with a separation of $1/6$ of the section width; and number 5 was positioned at $1/4$ of the section width.

2.5. Test procedure

The circular and square SR-CFST columns were first heated unloaded in the described electric furnace, since this condition is considered to be more conservative in the evaluation of the residual strength of concrete after heating [13–15]. For the thermal tests, both top and bottom surfaces were protected with fibre blankets to prevent heat loss. To guarantee that the embedded steel profile, in all of the tested specimens, had a significant reduction in its mechanical properties, the furnace temperature target was set to $1000\text{ }^{\circ}\text{C}$. As a result, due to the electric furnace power specifications, the heating times for all of the specimens were higher than 240 min. Once the target temperature was attained, the electric furnace was switched off and opened so that

the column cooled at ambient temperature. The time histories of the furnace and cross-sectional temperatures were registered during the heating and also part of the cooling process.

After the specimen had cooled down, the investigation continued with the compression test to obtain the residual strength of the SR-CFST column after heating. As presented in Fig. 5, a vertical testing frame with a hydraulic jack with capacity of 5000 kN was employed for that purpose. In Fig. 5, the setup of this mechanical test for one of the square SR-CFST columns is shown. The boundary conditions during the experiments for all of the tested stub columns were pinned–fixed (P–F) with a length of 400 mm. The mechanical response of each column was monitored by means of four LVDTs placed at the four sides of the column to register the top end axial displacement as well as to control slight deviations that may occur during loading. Additionally, two sets of strain gauges were attached to the four sides of the column in the longitudinal and transversal directions (see Fig. 5).

At the start of each experiment and right after the correct positioning of the specimen, the pertinent displacement control test was conducted. Thus, data from the four LVDTs were monitored to assure

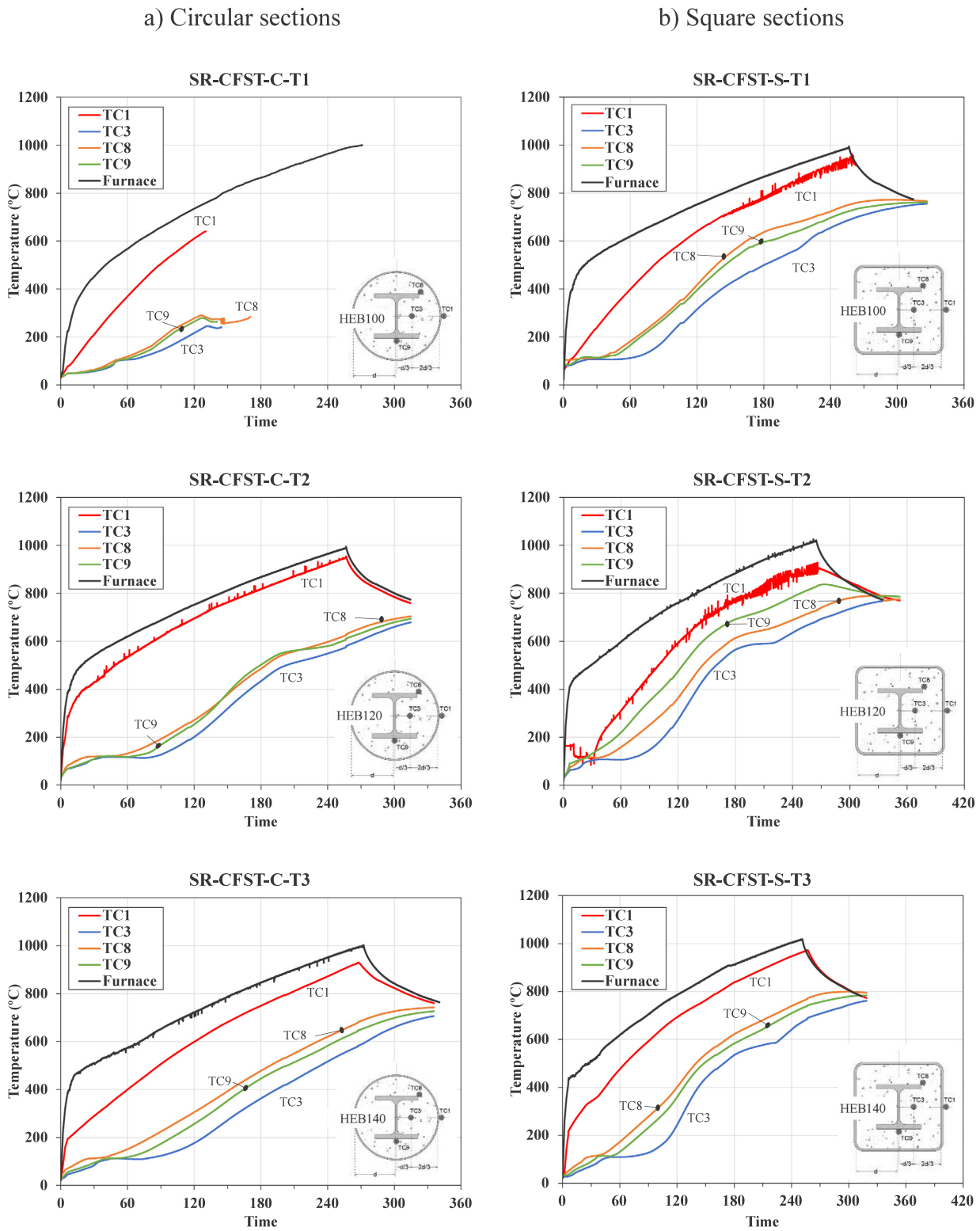


Fig. 6. Cross-sectional temperatures.

that the columns were, in fact, axially loaded and that the compression was uniformly applied. A displacement-controlled test was conducted with a loading rate of 0.1 mm/min. The load cell allowed to measure the applied load during the test which was recorded together with the evolution of the axial displacement of the columns, showing its shortening due to the applied load. From the data acquisition system, the time histories of the load and displacement rate were also recorded.

3. Analysis of experimental results

3.1. Cross-sectional temperatures

The time history of the cross-sectional temperatures monitored during the heating and part of the cooling process are shown in Fig. 6. Although data from the 12 thermocouples installed were recorded, for



Fig. 7. External surface of the columns after heating: (a) SR-CFST-C-T2; (b) SR-CFST-S-T2.

the sake of clarity only the temperatures of four of the thermocouples are displayed together with the evolution of the furnace temperature.

Due to a failure in the connection of some thermocouples to the data acquisition system when specimen SR-CFST-C-T1 was tested, temperatures are missing from 120 min on for TC1; from 150 min on for TC3 and TC9; and from approximately 180 min on for TC9.

As presented in Fig. 6, the effect of the thermal protection provided by the outer steel tube and the low thermal diffusivity of concrete can be perceived in the delay of temperature rise in the concrete core for both series. In general, temperatures are higher for the square SR-CFST columns than for the corresponding circular columns, which may be due to the effect of the section factor, since for the same cross-sectional area, the square sections present a higher exposed perimeter.

It can be seen that in the specimens SR-CFST-C-T3 and SR-CFST-S-T3, the embedded steel profile (HEB140) reaches higher temperatures than the other two types of sections. For the same external dimensions, the greater the embedded steel profile, the less the concrete cover that protects the profile.

The external surface of the steel tubes became dark burgundy and the characteristic orangey rust that usually covers the steel surface

disappeared. A close up of specimens SR-CFST-C-T2 and SR-CFST-S-T2 is shown in Fig. 7, where it can also be seen that part of the degraded outer thin layer of the steel tube sloughed off during heating. In Fig. 8a, the state of all of the tested columns after the heating is presented.

To illustrate the final state of all of the components of the columns after the tests, specimens SR-CFST-C-T1 and SR-CFST-S-T1 were selected for further examination and were cut longitudinally to analyse the embedded profile and the concrete core (see Fig. 9). It can be seen that the degraded concrete has a yellow colour in contrast to the undamaged concrete which still possess its original grey colour. With a dashed red line, the limit of the degradation area has been marked. As expected, this area includes the outer part of the concrete core and part of the concrete at the top of the column, due to the heat travelling to the upper part of the furnace during the heating. As can be seen in Fig. 6b for specimen SR-CFST-S-T1, the temperatures achieved at the last part of the heating test are between 600 °C and 800 °C. For temperatures higher than 600 °C a change in the concrete microstructure occurs producing the abovementioned change of colour.

3.2. Failure modes

In Fig. 8 the columns of the circular and the square series are shown after both the thermal (Fig. 8a) and the post-fire test (Fig. 8b) to have a general view of the state of the columns after the tests and directly visualize the changes in their physical state.

After the post-fire mechanical tests, the columns were highly damaged and cracked due to the high level of compression achieved during the test (see Fig. 8b). The columns at failure developed the characteristic elephant foot due to local buckling of the outer steel tube, especially the square specimens. As pointed out by Meng et al. [8], this phenomenon is caused by the different thermal expansion of the different materials and the uneven temperature field, which enables the steel tube to support the increasing axial load and yield. In the case of the tested columns, the outward bulges appeared near the top end of the columns, which may be due to the fact that it is on this end where the hole for water evaporation was drilled. Also, the ball joint of the load cell was located at this side, facilitating the folding of the steel tube closer to the top end.

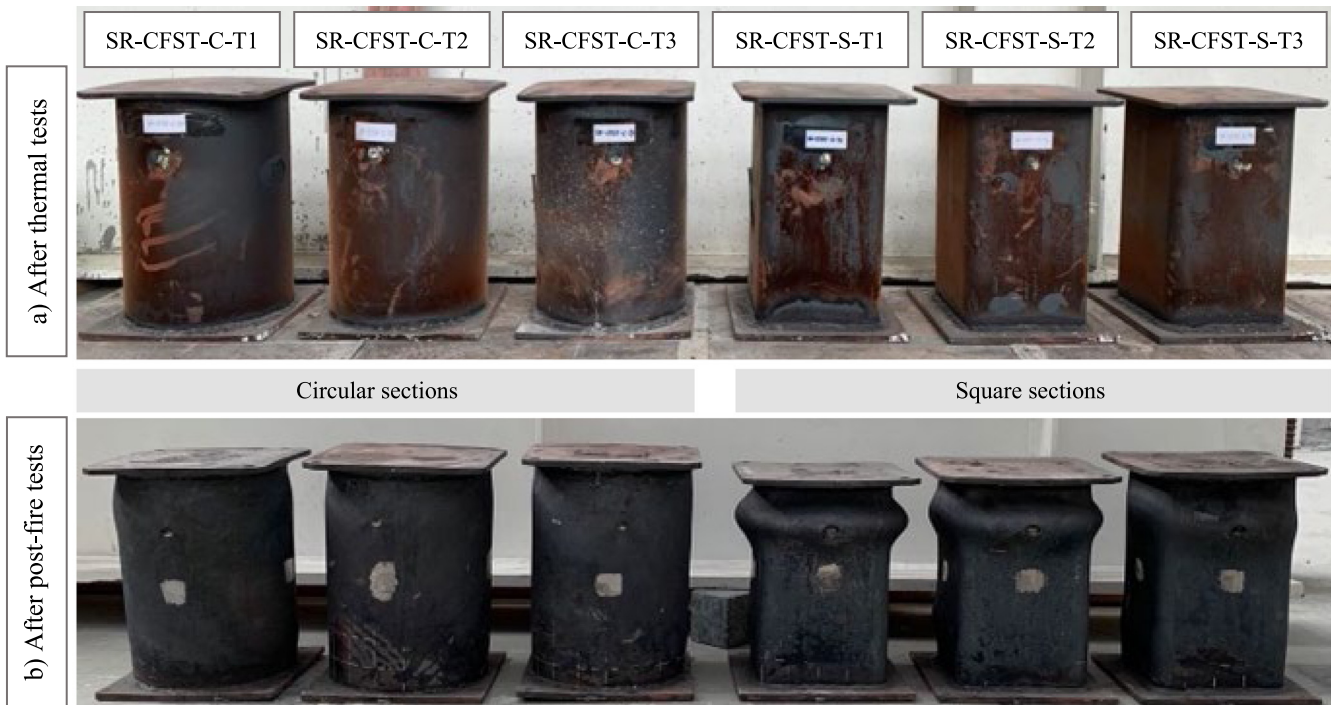


Fig. 8. Columns after the thermal and the post-fire mechanical test.

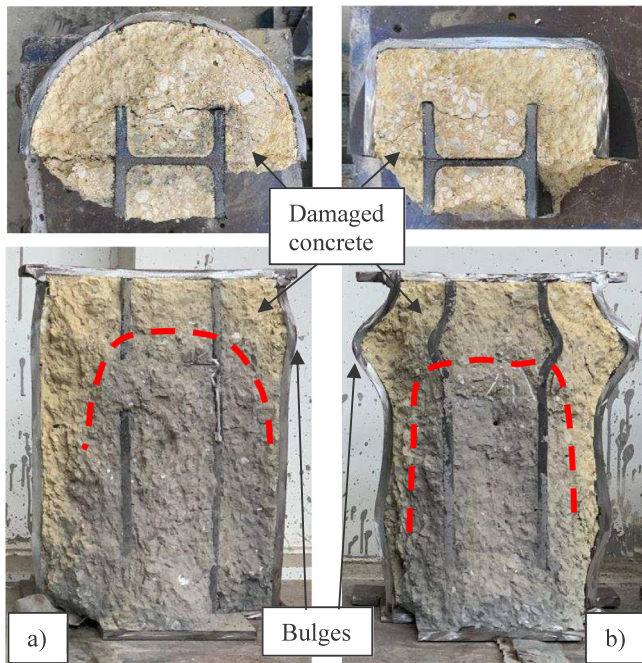


Fig. 9. Failure mode: (a) SR-CFST-C-T1; (b) SR-CFST-S-T1.

In general, the occurrence of the bulges was symmetrical and took place at the same location over the column length for the whole perimeter in both types of geometries (see Fig. 8b and Fig. 9). Right on the bulges, a gap appeared between the folded steel tube and the damaged concrete (see Fig. 9). Due to the maximum temperatures reached by the concrete, the bonding capacity of concrete was significantly reduced so the degraded concrete crumbled to the touch. This was also observed by Yang et al. [9] in their investigation since no plates were welded at the end of the tested columns so when the surfaces were being prepared for the mechanical test after the heating, it was observed that small bits and coarse aggregates scattered from the concrete. However, in this

experimental program, thanks to the welded steel plates, the concrete surface at the top end of the columns was practically intact and kept the planarity.

Another phenomenon observed in the tests was the apparition of shear slippage lines (see Fig. 10) that describe the plane of maximum tangential stress, with an angle of 45° with respect to the main compression stress direction (longitudinal axis). These lines appeared and generally started to grow when the applied load reached about 3000 kN (60%–75% of the maximum load), corresponding to the point when the outer steel tube entered the plastic stage, as will be later confirmed in the stress analysis presented in Section 3.3. The shear slippage lines continued to develop during the last part of the test and became greater until eventually the ultimate capacity of the columns was attained.

In Fig. 10 it can also be observed how a very thin superficial layer of the outer steel tube sloughs off. This is the mill scale (also known as calamine), a surface oxidation layer that is generated during the hot rolling process. This layer initially protects the steel tube when is in storage, but it is not very stable and eventually it peels off. In addition, its thermal expansion coefficient is smaller than that of the rest of the steel so it is very affected by the temperature gradients. Given that after heating it is more fragile, during the post-fire tests it sloughs off.

3.3. Stress analysis of the outer steel tube

The stress state of the outer steel tube during the load tests was measured using strain gauges, vertical and horizontal, at 0°, 90°, 180° and 270°, as shown in Fig. 11.

The strain gauge measurements registered during the load tests are provided in Fig. 12. For comparison purposes, only the results for the square specimens are shown. It is worth noting that in these graphs, positive strain implies contraction, while negative strain means elongation.

From these strain readings, the vertical (σ_v) and hoop (σ_h) stresses at the linear elastic range can be directly obtained by assuming a state of plane stress at the outer surface of the steel tube, based on Hooke's law:

$$\sigma_v = \frac{E_s}{1 - \nu_s^2} (\epsilon_v + \nu_s \epsilon_h)$$

$$\sigma_h = \frac{E_s}{1 - \nu_s^2} (\epsilon_h + \nu_s \epsilon_v)$$
(1)



Fig. 10. Shear slippage lines: (a) SR-CFST-C-T1 during the test; (b) SR-CFST-C-T2 bottom end close up.

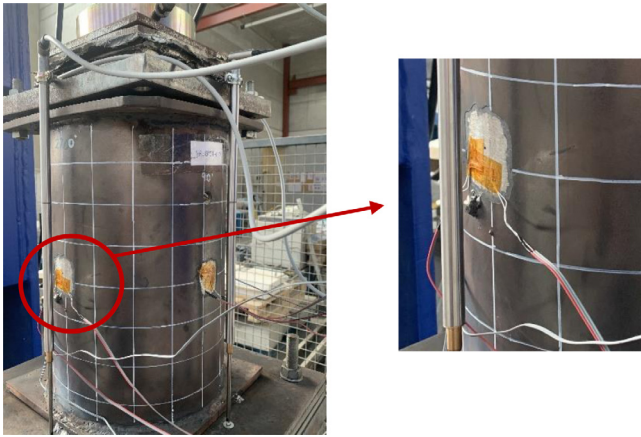


Fig. 11. Detailed view of the strain gauges attached to the outer steel tube surface.

where ε_v and ε_h are the longitudinal and transverse strain, respectively, ν_s is the Poisson's ratio of steel at the elastic range and E_s is the elastic modulus of steel.

Based on the elastic–plastic theory, the Von Mises equivalent stress can be computed, as given by:

$$\sigma_{eq,VM} = \frac{\sqrt{2}}{2} \sqrt{(\sigma_h - \sigma_v)^2 + \sigma_v^2 + \sigma_h^2} \quad (2)$$

where σ_v and σ_h are the longitudinal and transverse stress at the outer steel tube surface, respectively.

In the elastic–plastic range, however, the expressions given in Eq. (1) are not valid, thus the relevant stress–strain relations may be obtained based on an incremental procedure, as given in [16], where the tangent modulus of steel (E_s^t) may be updated at each strain increment:

$$E_s^t = \frac{(f_y - \sigma_{eq,VM})\sigma_{eq,VM}}{(f_y - f_p)f_p} E_s \quad (3)$$

as well as the Poisson's ratio:

$$\nu_{sp} = 0.217 \frac{\sigma_{eq,VM} - f_p}{f_y - f_p} + \nu_s \quad (4)$$

By applying the described procedure, the stress state of the outer steel tube during loading at the post-fire tests was obtained for the stub columns. It is worth mentioning that the referred mechanical properties of steel were assumed to be affected by the maximum temperature reached at the heating phase, that is, the corresponding post-fire residual factors were applied to f_p , f_y and E_s based on the maximum temperatures registered at the outer steel tube for each specimen.

Fig. 13 displays the evolution of the vertical (V) and hoop (H) stresses at the four studied orientations (0°, 90°, 180° and 270°) for specimen SR-CFST-S-T3. It is worth noting that in these graphs, positive stresses are compression stresses, while negative stresses refer to tensile stresses.

As it can be seen, at the initial stage of loading (elastic range), the vertical stresses increase linearly, while the transverse (hoop) stresses remain with a small value, increasing at a slower pace. As the axial load increases, the material enters into an elastic–plastic regime, where the slope of the load versus stress curves gradually reduces leading to the plastic stage, where both the vertical and horizontal stresses show a rapid development, indicating a possible effect of the lateral confinement stresses between the outer steel tube and the concrete core. This point occurs once the load level corresponding to a 60%–75% of the ultimate load (about 3000 kN) is reached. This is coincident with the visual observation of the development of the shear slippage lines at 45° relative to the longitudinal direction that was highlighted in Section 3.2, indicative of plastic failure in pure compression. In this

plastic stage, the stresses continue developing without a significant load increase, as it can be seen in the horizontal plateau in Fig. 14. A strain hardening stage can be recognized between 200 and 400 MPa, at the end of which the stresses tend to stabilize again, point where the steel tube failure takes hold. By computing the Von Mises equivalent stress at this point (see Fig. 14), values close to the post-fire ultimate strength of steel corresponding to the maximum temperature reached by the outer tube at the heating tests can be found.

As an example, specimen SR-CFST-S-T3 attained a maximum temperature at the outer tube of 989 °C, what according to [17] corresponds to a post-fire reduction coefficient of the ultimate strength of steel equal to 0.577, therefore $f_{u,post} = 0.577 \times f_{u,20} = 0.577 \times 680 \text{ MPa} = 392 \text{ MPa}$. From this point on, the outer steel tube is not capable to sustain the load anymore, thus being primarily sustained by the concrete core and the inner steel profile, until eventually the failure of the column occurs.

3.4. Force–displacement response

As can be seen in Fig. 15, the initial response was mostly linear elastic up to approximately 65%–70% of the peak load ($N_{post,exp}$), which is in concordance to the response observed by other authors [8]. The columns then entered the plastic range and the stiffness of the columns decreased gradually. Finally, the specimens achieved the peak load which kept constant for a significant period instead of presenting a sharp drop, showing the high ductility of the columns. Table 1 shows the values of the peak load registered during the experiments for all of the tested columns.

Note that in Fig. 15, for columns SR-CFST-C-T2 and SR-CFST-C-T3, the tests were manually paused due to the technical limitations of the vertical frame (5000 kN) and this fact did not allow to register the maximum load experimentally (see column $N_{post,exp}$ in Table 1).

In general, circular SR-CFST columns had higher peak loads than their square counterparts. For each series, the peak load at post-fire increased as the size of the embedded steel profile did, being the maximum values for the specimens with and embedded HEB140 (see Fig. 16).

3.5. Residual strength index

To quantify the loss of load bearing capacity experienced by the columns after being exposed to high temperatures, the Residual Strength Index (RSI) is calculated. The approach proposed by Han et al. [18] has been adopted, where RSI is defined as:

$$RSI = \frac{N_{post,exp}}{N_{u,0}} \quad (5)$$

where $N_{u,0}$ and $N_{post,exp}$ are the room temperature and experimental post-fire ultimate load respectively.

For the calculation of $N_{u,0}$, the equations given in Clause 6.7.3.2 of Eurocode 4 Part 1–1 [19] for evaluating the plastic resistance to compression of CFST sections are used and adapted to SR-CFST sections. Account for the inner steel profile will be done by adding its contribution to the plastic resistance of the composite cross-section in the summation of components, as previously proposed by Liew et al. [2].

In the case of square SR-CFST sections, confinement at room temperature is neglected. Therefore, $N_{u,0}$ may be calculated by adding the plastic resistances of its components, as given in Clause 6.7.3.2(1) of Eurocode 4 Part 1–1 [19]:

$$N_{u,0} = A_a f_{uo} + A_c f_c + A_{sp} f_{ui} \quad (6)$$

where A_a and f_{uo} are the cross-sectional area and the ultimate strength of the steel tube; A_c and f_c are the cross-sectional concrete area and the compressive cylinder strength of concrete; and A_{sp} and f_{ui} are the cross-sectional area and the ultimate strength of the embedded steel profile.

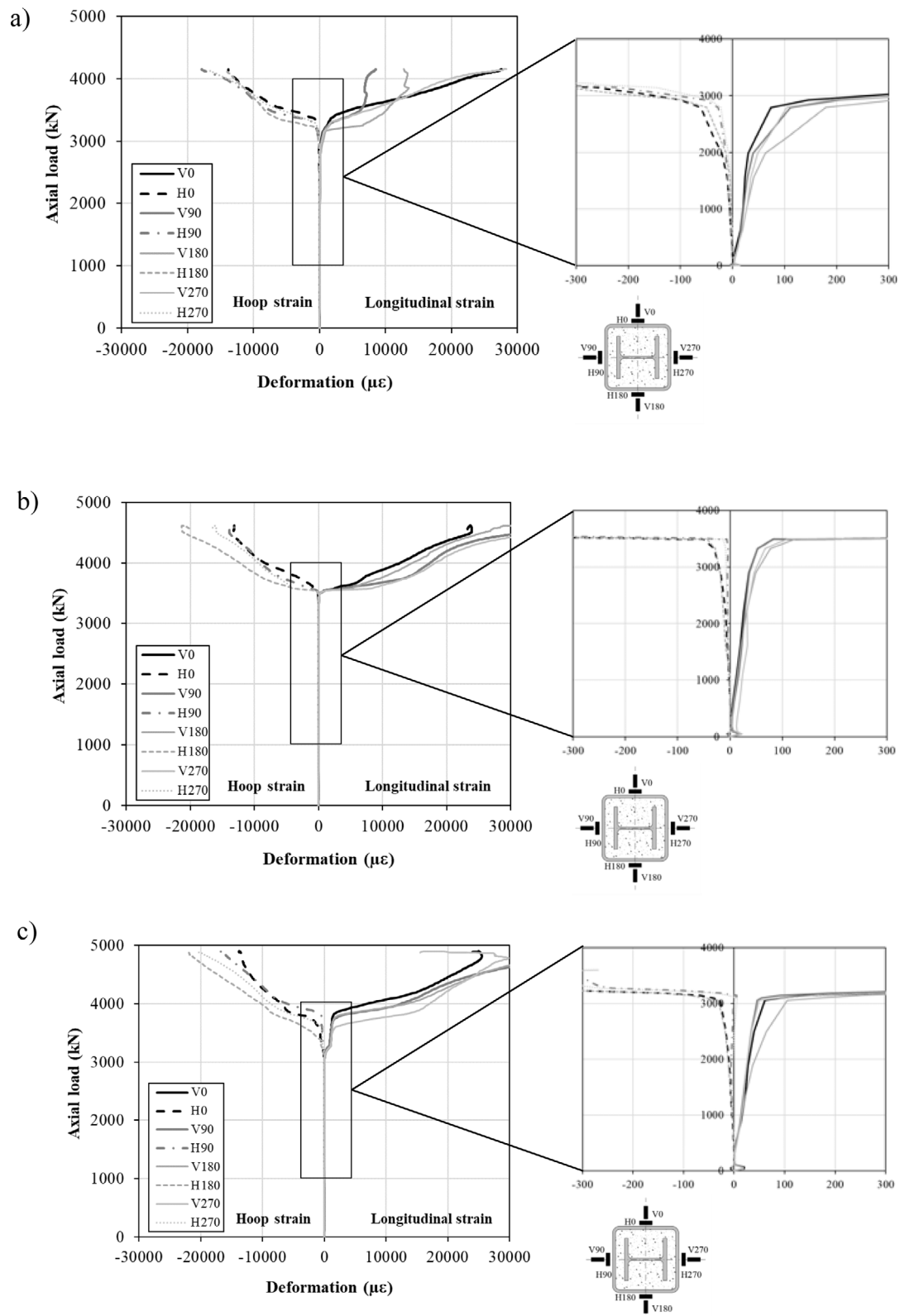


Fig. 12. Deformation state at the outer steel tube surface for the square columns: (a) SR-CFST-S-T1; (b) SR-CFST-S-T2; (c) SR-CFST-S-T3.

For circular columns, account may be taken of the increase in strength of concrete caused by confinement as stated in Clause 6.7.3.2 (6) of Eurocode 4 Part 1-1 [19], provided that the relative slenderness does not exceed 0.5 ($\bar{\lambda} < 0.5$) and a load eccentricity to diameter ratio less than 0.1 — what is the case of the studied columns. This is given

by:

$$N_{u,0} = \eta_a A_a f_{uo} + A_c f_c \left(1 + \eta_c \frac{t}{D} \frac{f_{uo}}{f_c} \right) + A_{sp} f_{ui} \quad (7)$$

where t is the wall thickness of the steel tube; D refers to the external diameter of the column; and η_a and η_c are the factors related to the

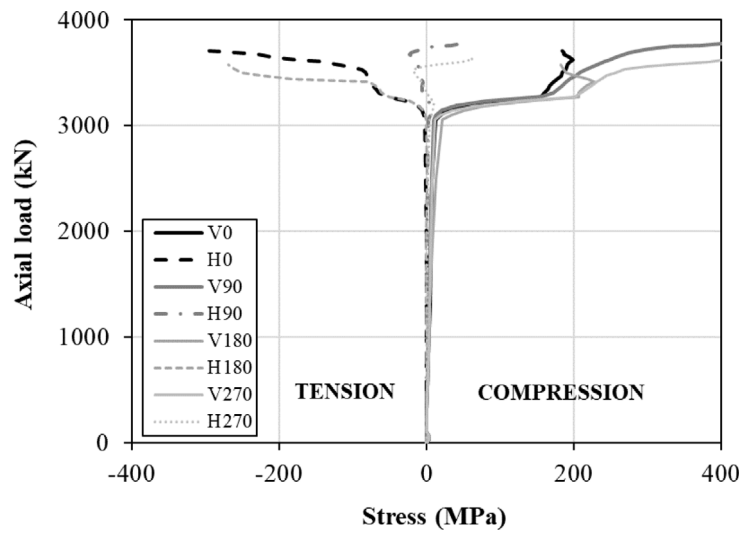


Fig. 13. Development of stresses at the outer steel tube surface for specimen SR-CFST-S-T3.

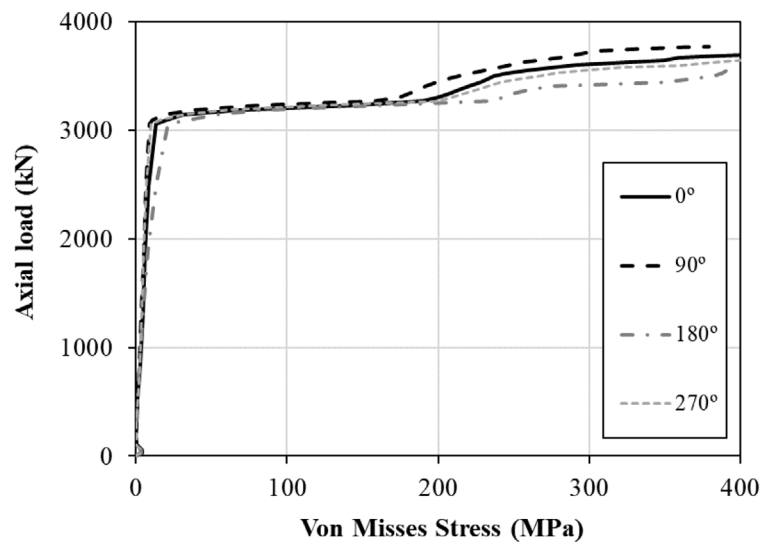


Fig. 14. Axial load versus Von Mises equivalent stress for specimen SR-CFST-S-T3.

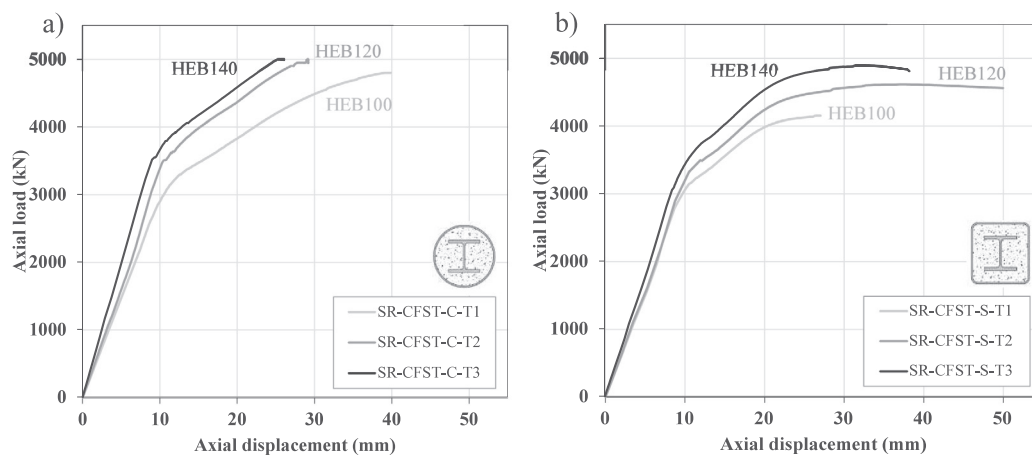


Fig. 15. Axial load-displacement curves: (a) circular sections; (b) square sections.

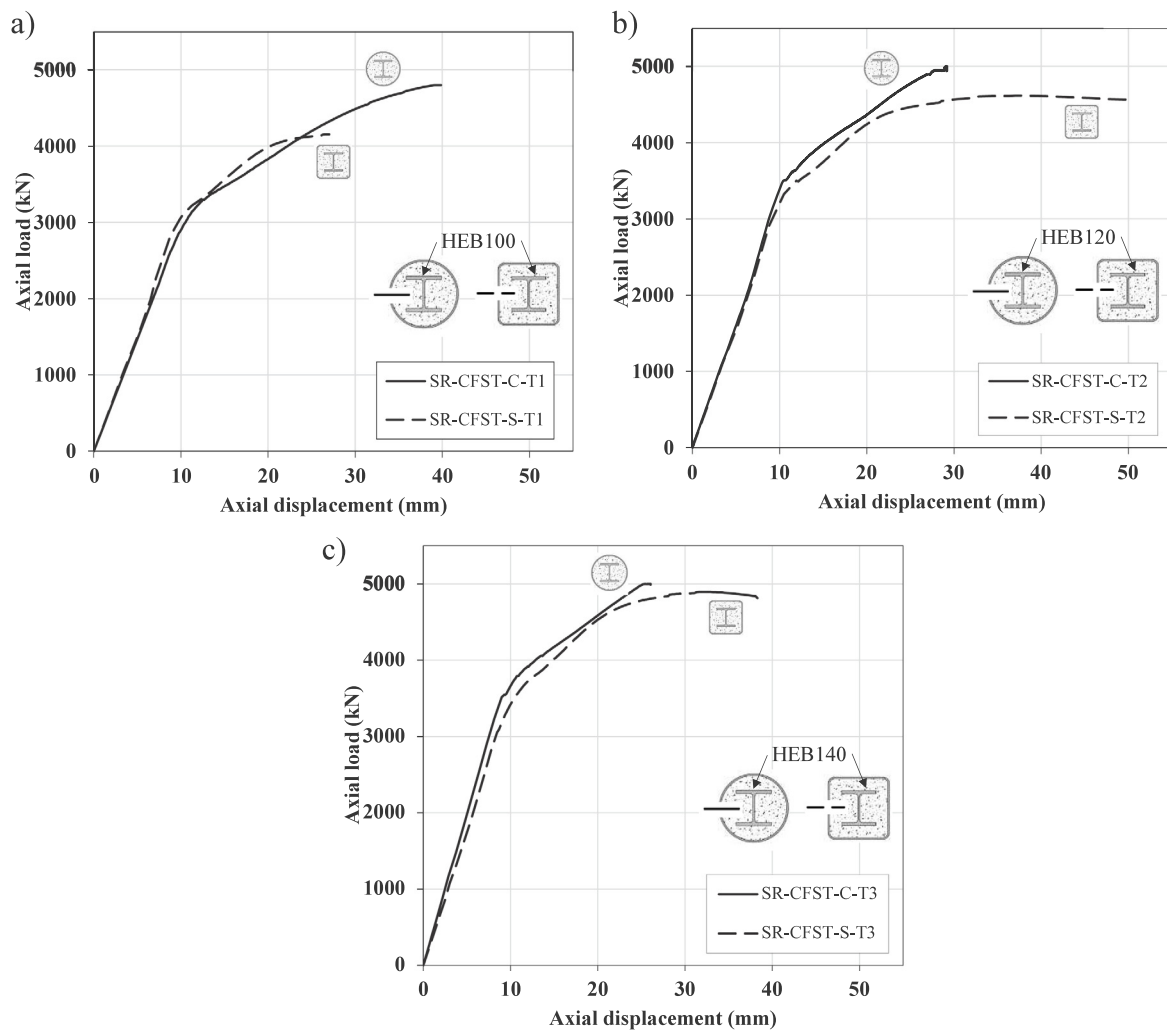


Fig. 16. Axial load–displacement curves for different embedded profiles: (a) HEB100; (b) HEB120; (c) HEB140.

confinement of concrete. For axially loaded members, these factors are given by:

$$\eta_a = 0.25 (3 + 2\bar{\lambda}) \tag{8}$$

$$\eta_c = 4.9 - 18.5\bar{\lambda} + 17\bar{\lambda}^2 \tag{9}$$



Note that Eurocode 4 Part 1–1 uses in these equations the design value for the yield strength of steel and for the concrete compressive strength, which in this investigation have been replaced for the actual values of the ultimate strength of steel and the actual concrete cylinder compressive strength derived from the material tests and reported in Table 1, as the aim is to obtain the ultimate capacity of the columns.

The calculated values for $N_{u,0}$ are presented in Table 2, together with the experimental values for the $N_{post,exp}$, which are shown again for comparison purposes.

For all of the tested columns, the values of the RSI are calculated as given in Eq. (5) and summarized in Table 2. For the circular SR-CFST columns, account for the confinement has been made. Note that for columns SR-CFST-C-T2 and SR-CFST-C-T3, the values of the RSI in Table 2 appear marked with * since they have been calculated assuming a $N_{post,exp}$ of 5000 kN, but the real values for those RSI would be slightly higher.

Fig. 17 illustrates the RSI values for both series. Generally, the RSI has the same order of magnitude for both circular and square columns, all of them around 0.55–0.60. The fact that the loss of capacity is similar for both shapes, implies that confinement, which

Table 2
Post-fire test results and RSI .

| | Specimen | $N_{u,0}$ (kN) | $N_{post,exp}$ (kN) | RSI |
|---|--------------|-------------------|------------------------|--------|
|  | SR-CFST-C-T1 | 8774 | 4799 | 0.547 |
| | SR-CFST-C-T2 | 9016 | >5000 | 0.554* |
| | SR-CFST-C-T3 | 9331 | >5000 | 0.536* |
|  | SR-CFST-S-T1 | 7547 | 4153 | 0.550 |
| | SR-CFST-S-T2 | 7856 | 4615 | 0.587 |
| | SR-CFST-S-T3 | 8245 | 4896 | 0.594 |

has been considered for the calculation of $N_{u,0}$ in circular columns, is still active at the post-fire situation. For the square SR-CFST columns, the difference between the RSI values of all of the tested columns is not very important (7.4% and 1.2% with respect to the lowest value of 0.55 corresponding to SR-CFST-S-T1). This can be due to the fact that the higher degradation of the larger inner steel profiles (less concrete cover to protect them from fire) compensates somehow with the greater cross-sectional area of the profile, thus leading to values of RSI quite similar for all of the tested specimens.

Note that the results analysed and the conclusions that may be drawn from them are valid for a heating time of 240 min to the t-T curve applied during these experiments. Further tests and the subsequent analyses should be conducted to evaluate the post-heating response and RSI under different fire models and heating times.

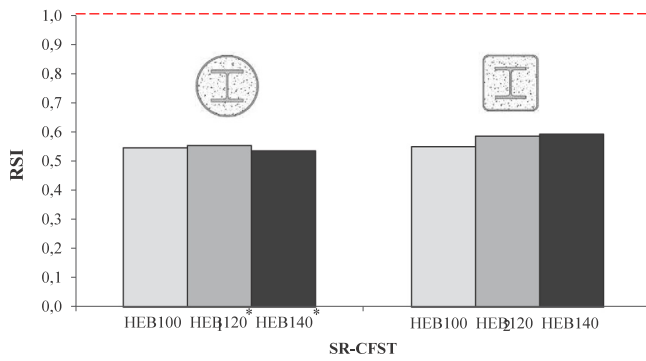


Fig. 17. Residual Strength Index (RSI).

4. Evaluation of the current design guidelines

In this section, an attempt to evaluate the residual load-bearing capacity of SR-CFST columns by means of the currently available design guidelines and considering the residual capacity of the materials after fire exposure is presented. For the residual factors of the materials, different proposals found in the literature are assessed.

At present, Eurocode 4 Part 1–2 [20] does not include any design recommendations to calculate the residual plastic resistance to compression of steel–concrete composite columns after being exposed to high temperatures. Therefore, in the absence of an established formula to do so, the expressions available in Clause 6.7.3.2 of Eurocode 4 Part 1–1 [19] for room temperature design will be used to evaluate the residual plastic resistance of SR-CFST columns, adapted to post-fire conditions by utilizing the residual material properties after fire exposure. Again, account for the inner steel profile will be done by adding its contribution in the summation of components in the post-fire situation, as already done for the room temperature evaluation of the plastic resistance of the composite cross-section [2]. Depending on the geometry of the sections (circular or square), effect of confinement will or will not be included in the calculations, which will be discussed at the end of this section.

Thus, following the same approach as Section 3.5 for the room temperature plastic resistance to compression of the cross-sections, Eqs. (6) and (7) will be adapted to post-fire conditions for evaluating the residual capacity of square and circular specimens.

Regarding the material properties, even though Eurocode 4 Part 1–2 [20] includes a formula in its Annex C to calculate the residual strength of concrete after fire exposure — available also in the last draft version of Eurocode 2 Part 1–2 (pr EN1992-1-2:2021-09) [21] —, there is still a lack of guidance regarding this matter for structural steel in the design codes.

Therefore, efforts have been made by several researchers to quantify the properties of structural steel after being affected by fire conditions. The different formulae available in the literature are assessed to test their level of accuracy in the prediction of the residual capacity of SR-CFST columns in contrast to the experimental results obtained in the present investigation.

The British Standard 5950-8:2003 [22] in its Annex B “re-use of steel after a fire”, Clause B.2.1, states that the mechanical properties of structural steels are not significantly affected until they reach temperatures higher than 600 °C. For micro-alloyed steels of grade S355 in particular, the British code states that it can be assumed that at least 75% of the strength is regained on cooling from temperatures above 600 °C.

In turn, Tao et al. [23] proposed a series of formulae to calculate the residual strength of both structural and reinforcing steel based on a statistical analysis of data from the literature. More recently, Molkens et al. [24] reviewed the post-fire tests for structural steel

available in the literature (718 tests in total). After the corresponding statistical analysis, these authors recommended a set of residual factors for normal, high-strength and very high-strength steel after exposure to elevated temperatures, which generally showed a sharp drop in the mechanical properties around 500–600 °C.

Finally, as part of the overarching project that encompasses this investigation, the post-fire residual strength of structural steel was also investigated [17]. In particular, coupons from different steel hollow sections were tested, obtaining the corresponding post-fire residual factors for varying temperatures, ranging from 20 to 1000 °C.

For the calculation of the residual plastic resistance, the cross-section discretization scheme presented in Fig. 18 is followed, with a clear differentiation of the three components of the section. The key parameter in this calculation is the maximum temperature reached by each material. For that reason, the embedded steel profile has been divided into two parts: flanges (more exposed to the heat source) and web (protected by the surrounding concrete). Also, given the non-uniform temperature field obtained in the concrete core when exposed to high temperatures, it has been divided in four concentric rings or layers as shown in Fig. 18. A representative temperature is assigned to each component or division of the cross-section. The values for these representative temperatures are the maximum values measured during the experiments presented in Section 3.2. The steel outer tube is assigned a temperature (θ_a) which ranges between 920 and 970 °C, depending on the experimental test. The temperatures for the flanges (θ_f) and the web (θ_w) of the inner steel profile range between 700 and 800 °C. For the concrete core, each ring or layer has its own representative temperature ($\theta_{c,i}$), which is associated to the peak temperature of the corresponding thermocouple (see Fig. 18).

Therefore, the plastic resistance to compression of the SR-CFST cross-sections after exposed to high temperatures will be obtained as follows:

Square sections (no confinement considered):

$$N_{u,post} = A_a f_{uo,post}(\theta_{a,max}) + \sum_{i=1}^4 A_{c,i} f_{c,post}(\theta_{c,i,max}) + A_w f_{ui,post}(\theta_{w,max}) + A_f f_{ui,post}(\theta_{f,max}) \quad (10)$$

where $A_{c,i}$ is the cross-sectional area of the i -th concrete ring or layer; $f_{c,post}$ is the ultimate concrete compressive strength affected by the corresponding residual factor for a maximum temperature $\theta_{c,i,max}$; A_w and A_f are the cross-sectional areas of the web and the flanges of the embedded steel profile; and $f_{uo,post}$ and $f_{ui,post}$ are the ultimate strength of the outer steel tube and the embedded steel profile affected by the corresponding residual factors for the maximum temperatures $\theta_{a,max}$, $\theta_{f,max}$ and $\theta_{w,max}$ respectively.

Circular sections (confinement effect included):

$$N_{u,post} = \eta_a A_a f_{uo,post}(\theta_{a,max}) + \sum_{i=1}^4 A_{c,i} f_{c,post}(\theta_{c,i,max}) \left(1 + \eta_c \frac{t}{D} \frac{f_{uo,post}(\theta_{a,max})}{f_{c,post}} \right) + A_w f_{ui,post}(\theta_{w,max}) + A_f f_{ui,post}(\theta_{f,max}) \quad (11)$$

where the average compressive strength of the concrete core after fire exposure to account for the confinement effect in the post-fire situation can be represented as:

$$\frac{f_{c,post}}{f_{c,post}} = \frac{\sum_{i=1}^4 A_{c,i} f_{c,post}(\theta_{c,i,max})}{A_c} \quad (12)$$

By applying the procedure explained above, the residual axial capacity of the six tested specimens is calculated and compared against the experimental values. The formula provided in Annex C of Eurocode 4 Part 1–2 [20] will be used to obtain the residual compressive strength of concrete after heating and cooling back to ambient temperature. In turn, for the steel parts (i.e. outer steel tube and embedded profile),

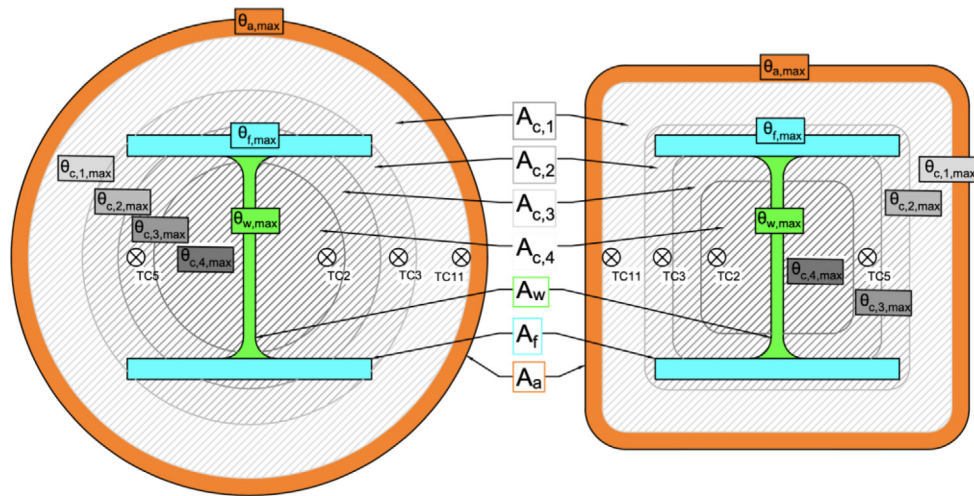




Fig. 18. Zones division of the cross-section.

Table 3
Post-fire residual plastic resistance for the SR-CFST columns calculated under different approaches for evaluating the residual factors.

| Specimen | $N_{post,exp}$ (kN) | $N_{calc,1}$ (kN) | $N_{calc,2}$ (kN) | $N_{calc,3}$ (kN) | $N_{calc,4}$ (kN) |
|---|---------------------|-------------------|-------------------|-------------------|-------------------|
|  SR-CFST-C-T1 | 4799 | 5785,9 | 6724,9 | 5118,1 | 4821,3 |
| SR-CFST-C-T2 | >5000* | 6077,3 | 7054,5 | 5446,3 | 5163,4 |
| SR-CFST-C-T3 | >5000* | 6447,0 | 7422,0 | 5632,4 | 5383,1 |
|  SR-CFST-S-T1 | 4153 | 5255.6 | 6202.1 | 4639.3 | 4368.2 |
| SR-CFST-S-T2 | 4615 | 5530.0 | 6483.9 | 4837.3 | 4556.4 |
| SR-CFST-S-T3 | 4896 | 5902.8 | 6831.2 | 4951.4 | 4726.9 |

Note: 1, British Standard [22]; 2, Tao et al. [23]; 3, Molkens et al. [24]; and 4, Pons et al. [17].



the four different approaches presented in this section (formulae and residual factors proposed by different authors) are assessed.

Therefore, in Table 3, the different calculated values for the post-fire residual plastic resistance of the tested columns are presented ($N_{calc,j}$), where the numbers at the subscripts j correspond to: 1, British Standard [22]; 2, Tao et al. [23]; 3, Molkens et al. [24]; and 4, Pons et al. [17]. Column $N_{post,exp}$ in Table 3 displays the values of the experimental capacity of the specimens after fire exposure (taken from Section 3.4), which is used as a reference for the assessment of the different approaches.

In Table 4, the calculated values are compared with the experimental results using the relation $N_{post,exp}/N_{calc,j}$. Note that a value greater than one for the error indicates a conservative prediction, while a value lower than one stands for a no conservative prediction. The mean error and the standard deviation (SD) obtained for each approach are also summarized in Table 4. Note that, once more, the values of columns SR-CFST-C-T2 and SR-CFST-C-T3 appear marked with * in Table 4 since they have been calculated assuming a $N_{post,exp}$ of 5000 kN. These values have also been neglected in the calculation of the mean and SD of the prediction errors.

Although all of the studied proposals only consider a significant reduction of the steel mechanical properties after being exposed to temperatures higher than 500–600 °C, some differences can be found in their predictions. It can be seen that both the British Standard [22] approach ($N_{post,exp}/N_{calc,1}$) and the residual factors proposed by Tao et al. [23] ($N_{post,exp}/N_{calc,2}$) greatly overestimate the residual plastic resistance (average error well below 1), being the second one the least accurate of all of the studied approaches with a mean error of 0.70 (30% overestimation). In turn, the set of residual factors proposed by Molkens et al. [24] provides a better agreement between the experimental and the theoretical values ($N_{post,exp}/N_{calc,3}$) with a mean

Table 4
 $N_{post,exp}/N_{calc,j}$ for the different approaches compared.

| Specimen | $N_{post,exp}/N_{calc,1}$ | $N_{post,exp}/N_{calc,2}$ | $N_{post,exp}/N_{calc,3}$ | $N_{post,exp}/N_{calc,4}$ |
|---|---------------------------|---------------------------|---------------------------|---------------------------|
|  SR-CFST-C-T1 | 0.83 | 0.71 | 0.94 | 1.00 |
| SR-CFST-C-T2 | 0.82* | 0.71* | 0.92* | 0.97* |
| SR-CFST-C-T3 | 0.78* | 0.67* | 0.89* | 0.93* |
|  SR-CFST-S-T1 | 0.79 | 0.67 | 0.90 | 0.95 |
| SR-CFST-S-T2 | 0.83 | 0.71 | 0.95 | 1.01 |
| SR-CFST-S-T3 | 0.83 | 0.72 | 0.99 | 1.04 |
| Mean | 0.82 | 0.70 | 0.94 | 1.00 |
| SD | 0.02 | 0.02 | 0.04 | 0.04 |

error of 0.94. The comparison shows that the set of residual factors proposed by Pons et al. [17] ($N_{post,exp}/N_{calc,4}$) gives the most accurate predictions, with an average value of the prediction error equal to 1.00 and a reduced scatter (standard deviation 0.04). This proposal assumes in fact a more accurate and progressive loss of capacity of steel, in contrast with other approaches that basically discriminate between temperatures above or below 500–600 °C. Therefore, the set of residual factors proposed by Pons et al. [17] is recommended to be used in combination with Eq. (11) for the calculation of the post-fire residual compression resistance of SR-CFST columns. It should be noted that the proposal described in this section it is just a preliminary approach developed with a very limited number of experiments. Given the reduced number of experimental results, the conclusions of this analysis cannot be considered to be definitive. For the development and validation of a solid proposal, more data will be needed, from both experiments and validated numerical models able to capture the response of the columns. Therefore, the predictions should then be taken with caution.

It should also be highlighted that the calculated values for the circular specimens include the effect of confinement, which has been considered in the contribution of the concrete part to the cross-sectional capacity as given in Eq. (11). If confinement would have been neglected for the circular specimens, the results would arise very low predictions of the ultimate load: as an example, for column specimen SR-CFST-C-T1 the predicted value would be 3743.4 kN with the proposed set of residual factors from Pons et al. [17] (leading to a 28% error). This result seems to confirm that confinement is still active at the post-fire situation and contributes to increase the ultimate load of the circular columns to a certain extent, conclusion which should be further confirmed by means of a deeper study through parametric studies.

5. Summary and conclusions

In this experimental investigation, the residual axial compression capacity of stub SR-CFST columns in a post-fire situation has been studied. For that purpose, a series of six SR-CFST specimens were tested, three of them with circular section and another three with square section. For comparison purposes, the circular and square steel tubes were selected so that the amount of steel used at the outer tube was similar (with a maximum difference of a 2.51%). In order to reproduce the situation of a post-fire event, the columns were in a first stage uniformly heated inside an electric furnace and, after cooling down to ambient, they were tested to failure in a vertical frame by applying an increasing axial load. The evolution of the temperatures at the relevant points of the cross-section was registered during the thermal tests by means of an arrangement of thermocouples, while the axial load versus displacement histories and strain measurements at the outer steel tube surface were captured during the loading tests, which were analysed to understand the stress development and the failure patterns at the post-fire situation. The analysis of the experimental results allowed reaching some relevant conclusions on the post-fire behaviour of SR-CFST columns:

- Temperatures registered during the heating tests were generally higher for the square SR-CFST sections than for their circular counterparts, which are attributed to the higher section factor of square columns. This causes a faster degradation of the square columns, leading to lower ultimate loads after fire exposure.
- For the same external dimensions, specimens with a larger embedded steel profile experienced a higher temperature rise at the inner parts of the section, as the amount of concrete cover protecting the steel profile from the heat source is lower. However, this effect compensates with the higher dimensions of the inner profile and thus higher axial capacity.
- The SR-CFST stub columns showed a high ductility after heating, with the circular specimens reaching higher peak loads than their square counterparts. For each series, the peak load at post-fire increased with the size of the embedded steel profile.
- The evaluation of the *RSI* showed that the loss of capacity after fire was similar for circular and square SR-CFST columns, and that the influence of the size of the embedded steel profile was not significant in the rate of capacity loss. This analysis also pointed out that, for circular columns, confinement may still be active at the post-fire situation, contributing to increase their ultimate load.

The currently available design rules were revised, finding that there is still a lack on guidance regarding the post-fire evaluation of steel-concrete composite columns and in particular for SR-CFST sections. In the absence of a method to do so, the equations for evaluating the axial capacity of CFST sections at room temperature in Eurocode 4 Part 1–1 were adapted to account for the residual capacity of the materials after fire exposure. Different proposals found in the literature for the residual factors of steel and concrete after fire exposure were assessed, being the proposal from Pons et al. [17] the one that aroused the best predictions. The results of this comparison seemed also to confirm that confinement is still active at the post-fire situation in the circular SR-CFST sections and therefore its effect should be accounted for in the evaluation of its residual capacity after fire exposure. The proposed post-fire design equations and residual factors showed a good agreement with the experimental results, although given the limited number of available tests, further parametric studies should be conducted in order to strengthen these conclusions.

CRedit authorship contribution statement

D. Medall: Writing – original draft, Methodology, Investigation, Formal analysis, Conceptualization. **C. Ibáñez:** Writing – original draft, Methodology, Investigation, Formal analysis, Conceptualization. **V. Albero:** Methodology, Investigation, Conceptualization. **A. Espinós:**

Writing – original draft, Project administration, Methodology, Investigation, Funding acquisition, Conceptualization. **M.L. Romero:** Supervision, Project administration, Investigation, Funding acquisition, Conceptualization.

Declaration of competing interest

The authors declare the following financial interests/personal relationships which may be considered as potential competing interests: Ana Espinos reports financial support was provided by Agencia Estatal de Investigación. David Medall reports financial support was provided by Agencia Estatal de Investigación.

Data availability

Data will be made available on request.

Acknowledgements

The authors would like to express their sincere gratitude for the help provided through the Grant PID2019-105908RB-I00 and for the first author's pre-doctoral contract through the Grant PRE2020-093106 funded by MCIN/AEI/10.13039/501100011033 and by "ESF Investing in your future". The authors are deeply grateful to Dr Enrique Serra for his help and assessment to prepare and conduct the experiments and Dr Andrés Lapuebla-Ferri and Dr David Pons for their help in conducting the material tests. Finally, the authors would like to acknowledge the funding for open access charge from CRUE-Universitat Politècnica de València.

References

- [1] M.L. Romero, A. Espinós, C. Renaud, G. Bihina, P. Schaumann, I. Kleiboemer, Fire Resistance of Innovative and Slender Concrete Filled Tubular Composite Columns (FRISCC). Final Report. Catalogue Number KI-NA-28082-EN-N, RfCS Publications, Brussels, 2016.
- [2] J. Liew, M. Xiong, Design Guide for Concrete Filled Tubular Members with High Strength Materials To Eurocode 4, Research Publishing, Singapur, 2015.
- [3] D. Medall, A. Espinós, V. Albero, M.L. Romero, Simplified proposal for the temperature field of steel-reinforced CFST columns exposed to fire, Eng. Struct. 273 (2022) 115083, <http://dx.doi.org/10.1016/j.engstruct.2022.115083>.
- [4] Dotrepe J. Claude, Chu T. Binh, R. Eng, Franssen J. Marc, Steel hollow columns filled with self-compacting concrete under fire conditions, 2010.
- [5] F.-Q. Meng, M.-C. Zhu, G.C. Clifton, K.U. Ukanwa, JBP Lim, Performance of square steel-reinforced concrete-filled steel tubular columns subject to non-uniform fire, J. Constr. Steel Res. 166 (2020) <http://dx.doi.org/10.1016/j.jcsr.2019.105909>.
- [6] Meng Fan-Qin, Zhu Mei-Chun, G. Charles Clifton, Kingsley U. Ukanwa, James B.P. Lim, Fire performance of edge and interior circular steel-reinforced concrete-filled steel tubular stub columns, Steel Compos. Struct. 41 (2021) 115–122.
- [7] W.J. Mao, W. da Wang, K. Zhou, E.F. Du, Experimental study on steel-reinforced concrete-filled steel tubular columns under the fire, J. Constr. Steel Res. 185 (2021) 106867, <http://dx.doi.org/10.1016/j.jcsr.2021.106867>.
- [8] F. Meng, M.-C. Zhu, B. Mou, B. He, Residual strength of steel-reinforced concrete-filled square steel tubular (SRCFST) stub columns after exposure to ISO-834 standard fire, Int. J. Steel Struct. 19 (2019) 850–866, <http://dx.doi.org/10.1007/s13296-018-0174-z>.
- [9] X. Yang, C. Tang, Y. Chen, T.-Y. Qiao, Compressive behavior of steel-reinforced concrete-filled square steel tubular stub columns after exposure to elevated temperature, Eng. Struct. 204 (2020) 110048, <http://dx.doi.org/10.1016/j.engstruct.2019.110048>.
- [10] EN 10219-1:2007, Cold formed welded structural hollow sections of non-alloy and fine grain steels - part 1: Technical delivery conditions, 2007.
- [11] EN 10025-1:2006, Hot rolled products of structural steels - part 1: General technical delivery conditions, 2006.
- [12] CEN. EN. 1992-1-1, Eurocode 2: Design of Concrete Structures, Part 1.1: General Rules and Rules for Buildings, Comité Européen de Normalisation, Brussels, Belgium, 2004.
- [13] K.D. Hertz, Concrete strength for fire safety design, Mag. Concr. Res. 57 (2005) 445–453, <http://dx.doi.org/10.1680/mac.2005.57.8.445>.
- [14] J. Huo, G. Huang, Y. Xiao, Effects of sustained axial load and cooling phase on post-fire behaviour of concrete-filled steel tubular stub columns, J. Constr. Steel Res. 65 (2009) 1664–1676, <http://dx.doi.org/10.1016/j.jcsr.2009.04.022>.

- [15] F. Liu, L. Gardner, H. Yang, Post-fire behaviour of reinforced concrete stub columns confined by circular steel tubes, *J. Constr. Steel. Res.* 102 (2014) 82–103, <http://dx.doi.org/10.1016/J.JCSR.2014.06.015>.
- [16] S. Zhang, L. Guo, Z. Ye, Y. Wang, Behavior of steel tube and confined high strength concrete for concrete-filled RHS tubes, *Adv. Struct. Eng.* 8 (2005) 101–116, <http://dx.doi.org/10.1260/1369433054037976>.
- [17] D. Pons, A. Lapuebla-Ferri, M.L. Romero, Post-fire residual strength and ductility of structural steels from hollow sections, *Ce/Papers* 5 (2022) 458–466, <http://dx.doi.org/10.1002/cepa.1777>.
- [18] L.H. Han, J.S. Huo, Y.C. Wang, Compressive and flexural behaviour of concrete filled steel tubes after exposure to standard fire, *J. Constr. Steel. Res.* 61 (2005) 882–901, <http://dx.doi.org/10.1016/j.jcsr.2004.12.005>.
- [19] CEN. EN 1994-1-1, Eurocode 4: Design of Composite Steel and Concrete Structures. Part 1.1: General Rules and Rules for Buildings. Brussels, Comité Européen de Normalisation, Belgium, 2004.
- [20] CEN. EN 1994-1-2, Eurocode 4: Design of Composite Steel and Concrete Structures. Part 1.2: General Rules - Structural Fire Design, Comité Européen de Normalisation, Brussels, Belgium, 2005.
- [21] CEN/TC250/SC2 N1897, Stable version pren 1992-1-2:2021-09. Eurocode 2: Design of concrete structures - part 1-2: General rules - structural fire design, 2021.
- [22] British Standards Institution (BSI), BS 5950-8:2003 structural use of steelwork in building. British standards, 2003, p. 8.
- [23] Z. Tao, X.-Q. Wang, B. Uy, Stress-strain curves of structural and reinforcing steels after exposure to elevated temperatures, *J. Mater. Civ. Eng.* 25 (2013) 1306–1316, [http://dx.doi.org/10.1061/\(ASCE\)MT.1943-5533.0000676](http://dx.doi.org/10.1061/(ASCE)MT.1943-5533.0000676).
- [24] T. Molkens, K.A. Cashell, B. Rossi, Post-fire mechanical properties of carbon steel and safety factors for the reinstatement of steel structures, *Eng. Struct.* 234 (2021) 111975, <http://dx.doi.org/10.1016/J.ENGSTRUCT.2021.111975>.